applied sciences

MDPI

Article

A Case Study of the Radon Hazard at the Boundary of a Coal Minefield

Timofey Leshukov [1,*], Konstantin Legoshchin [1] and Aleksey Larionov [2]

[1] Department of Geology and Geography, Institute of Biology, Ecology and Natural Resources, Kemerovo State University, 6 Krasnaya Street, 650000 Kemerovo, Russia; geology@kemsu.ru
[2] Department of Genetics and Fundamental Medicine, Institute of Biology, Ecology and Natural Resources, Kemerovo State University, 6 Krasnaya Street, 650000 Kemerovo, Russia; larionov@kemsu.ru
* Correspondence: tvleshukov@kemsu.ru

Abstract: The main purpose of this study is to assess the radon hazard in areas near the boundary of a coal mine. Our assessment included an analysis of the soil's radon volume activity (VAR) and radon flux density (RFD), as well as their spatial characteristics and correlations with other factors. The soil VAR varies in the range from 3477.7 to 17,520 Bq/m^3 (mean value 9786.9 $\pm$ 474.9 Bq/m^3), and RFD from 10 to 160 mBq·m^{-2}·s^{-1} with a mean value of 59.76 $\pm$ 2.45 mBq·m^{-2}·s^{-1}. The RFD parameter is spatially clustered ($p \leq 0.01$). No significant differences between RFD and soil VAR were found, both inside and outside the minefield areas ($p \geq 0.05$). However, we suggest considering the entire studied space of the minefield boundaries and surroundings to be radon-hazardous. This contributes to the understanding of the radon hazard of coal mines for ground structures both in the mine area and in its surroundings.

Keywords: coal mine; soil radon; radon flux density; tectonic faults; radon exhalation; Kuznetsk coal basin

check for updates

Citation: Leshukov, T.; Legoshchin, K.; Larionov, A. A Case Study of the Radon Hazard at the Boundary of a Coal Minefield. *Appl. Sci.* **2023**, *13*, 13188. https://doi.org/10.3390/app132413188

Academic Editor: Jan Yperman

Received: 31 October 2023
Revised: 21 November 2023
Accepted: 27 November 2023
Published: 12 December 2023

Copyright: © 2023 by the authors. Licensee MDPI, Basel, Switzerland. This article is an open access article distributed under the terms and conditions of the Creative Commons Attribution (CC BY) license (https://creativecommons.org/licenses/by/4.0/).

1. Introduction

Radon is a radioactive natural element that is an inert, heavier-than-air gas and well soluble in water at standard conditions. The three natural radon isotopes are ^{222}Rn ($T_{1/2}$ = 3.82 day), ^{220}Rn (55.6 $T_{1/2}$ = s), and ^{219}Rn ($T_{1/2}$ = 3.96 s). These isotopes are intermediate elements in a radioactive decay chain of the natural elements ^{238}U, ^{232}Th, and ^{235}U, respectively. The radon level is determined by the maternal element level and local features, such as soil porosity and moisture, which alleviate radon gas spreading and reaching the surface. In addition, rocks used as construction materials with a high concentration of uranium/thorium can be a source of radon. Due to a short half-life, the radon concentration remains low in the atmosphere, but radon accumulation in underground mines, basements, and ground floors (e.g., a lower air pressure in homes compared with the outdoors in a cold climate facilitates radon transport from the soil surface) make it one of the most dangerous carcinogenic factors for the human population. The indoor radon level can be 5–10 times higher than the outdoor level. Inhaling radon provides about 50 percent of the average human ionizing radiation exposure dose and provides a significant additional risk of lung cancer in the human population [1,2]. Inhaled radon and its short-living progeny emit high-LET (linear energy transfer) alpha particles, inducing local exposure and leading to DNA damage in airways and alveolar tissue [3,4]. The World Health Organization reports that about 3–14% of lung cancer cases are provoked by radon, and every excessive 100 Bq/m^3 increases the risk by 16% [5]. Radon exposure risk occurs as ionizing radiation, is not dependent on gender and age, and can be modified by smoking and maybe from ingesting other air particle matter, which can absorb radon progeny isotopes ^{218}Po, ^{214}Pb, and ^{214}Bi.

Radon extraction from soils can vary drastically within one area with a homogeneous geological structure. This variation is caused by soil porosity, water saturation, and temperature. Also, faults and rock fractures caused naturally by technogenic activity create additional ways for radon to migrate to the surface [6–10]. All rocks can be classified as fissure–pore formations. Radon is emitted from rocks into pores and crack spaces, and some of it goes into adsorbent and absorbent. Tectonic disturbance areas exhibit a greater volume of fissure–pore space, facilitating the accumulation of noteworthy amounts of liquids and gases, such as radon. Radon is subsequently transported from these voids to the surface by means of diffusion, convection, and other forces. Accompanying gases, particularly methane and hydrogen, play a crucial role in stimulating the migration rate of radon. Alterations to the stress–strain state of rocks cause significant changes to the volume of the pore–crack space. The compression zone results in a decrease, while in the tension zone, an increase occurs. Consequently, this leads to a low volume of radon and a low capability to move to the surface along the fault zone. Active faults generally exhibit significant variation in the radon field above them, while inactive faults tend to be more stable or not evident at all [11–15]. Previous research has shown that an area with significant soil radon concentration, which emanates to the surface, forms above the fault zone. This radon concentration may exceed the area of rock crushing that accompanies tectonic disturbances [16].

The territories where underground workings are located are characterized by the formation of zones of geological disturbances of different scales and uneven subsidence of the ground. This leads to the formation of channels and cavities, contributing to radon escaping to the surface.

Underground coal mines can substantially shift the radiological parameters of the adjacent part of the lithosphere and other shells [17–20]. The crustal areas where underground workings are located are characterized by an increased potential for the development of neotectonic processes. It can be assumed that these effects are more intense on the periphery of the excavated underground space. There, as a result of the subsidence of the excavation roof in depth, additional zones of tectonic disturbance under tensile conditions are likely to be formed. In addition, the activation of ancient faults that are located nearby is also possible. These structural changes in the rock can potentially lead to the formation of additional radon transport channels. Such effects even occur in areas composed of weakly radioactive rocks. If residential buildings are located in territories within the geodynamic influence of mines, it can lead to the deterioration of radiological safety conditions for the resident population [21,22]. It is suggested that the influence of underground mines on the dynamics of gas transport to the surface extends beyond the mined areas [16,18,23]. However, the quantitative parameters of this influence remain insufficiently studied.

The assessment of the radon hazard of mining areas and their surroundings is very important in areas of intensive mining activity. Kuznetsk coal basin is considered to be one of the largest coal mining regions in Russia, with a high specialization of the economy of most cities on mining.

Residential buildings that are situated on soils with a significant radon concentration in the underground atmosphere or a high emanation to the surface are a grave hazard to the population. The release of radon from the soil into living spaces occurs due to the "pump effect", which is reliant on a temperature difference [24,25]. During winter, radon entry speeds up with the rise in temperature difference between the structure and the geological environment. High soil radon levels caused by faults in the Earth's crust and mining activities can increase the risk of developing cancer for residents of the Kuznetsk coal basin.

Significant parts of the territories of coal mining towns have been exposed to the effects of underground coal mining, which has led to the formation of high-risk zones for radon emission. Previously, we detected significant levels of radon flux density (RFD) and volumetric radon activity (VAR) in dwellings above mines [21,22]. Similar situations are being studied in coal mining areas in Poland, the United Kingdom, China, and other

countries [17–20,26,27]. A radonometric assessment of mining areas is necessary because exposure to radon from mines may extend beyond the boundaries of the minefield area. Moreover, mining frequently extends to the edges of the fractured zone in disturbance zones bordering the mine. These rock fracturing zones are natural transport channels that degas the upper part of the Earth's crust, including radon. In this study, we aim to examine the radon hazard at the boundary of a coal minefield.

2. Materials and Methods

2.1. Study Location

The study area was located in the Kuznetsk coal basin, in the territory of the Salair–Altai–Irtysh fold. The soils within this site are characterized by leached chernozem. The variation in altitude relief is 40 m, with the average height above sea level being 240 m.

Figure 1 illustrates the study area, pinpointing the sites of observation, as well as the areas affected by both old and new coal mining activities. Figure 1 also features the tectonic fault location and its associated disturbance zone. Kuzbass is known for its shift in the stress–strain condition of the lithosphere, which results in technogenic seismic activities [28]. This situation can lead to a remarkable variation in radon fields, particularly in areas with tectonic disturbances due to their activation.

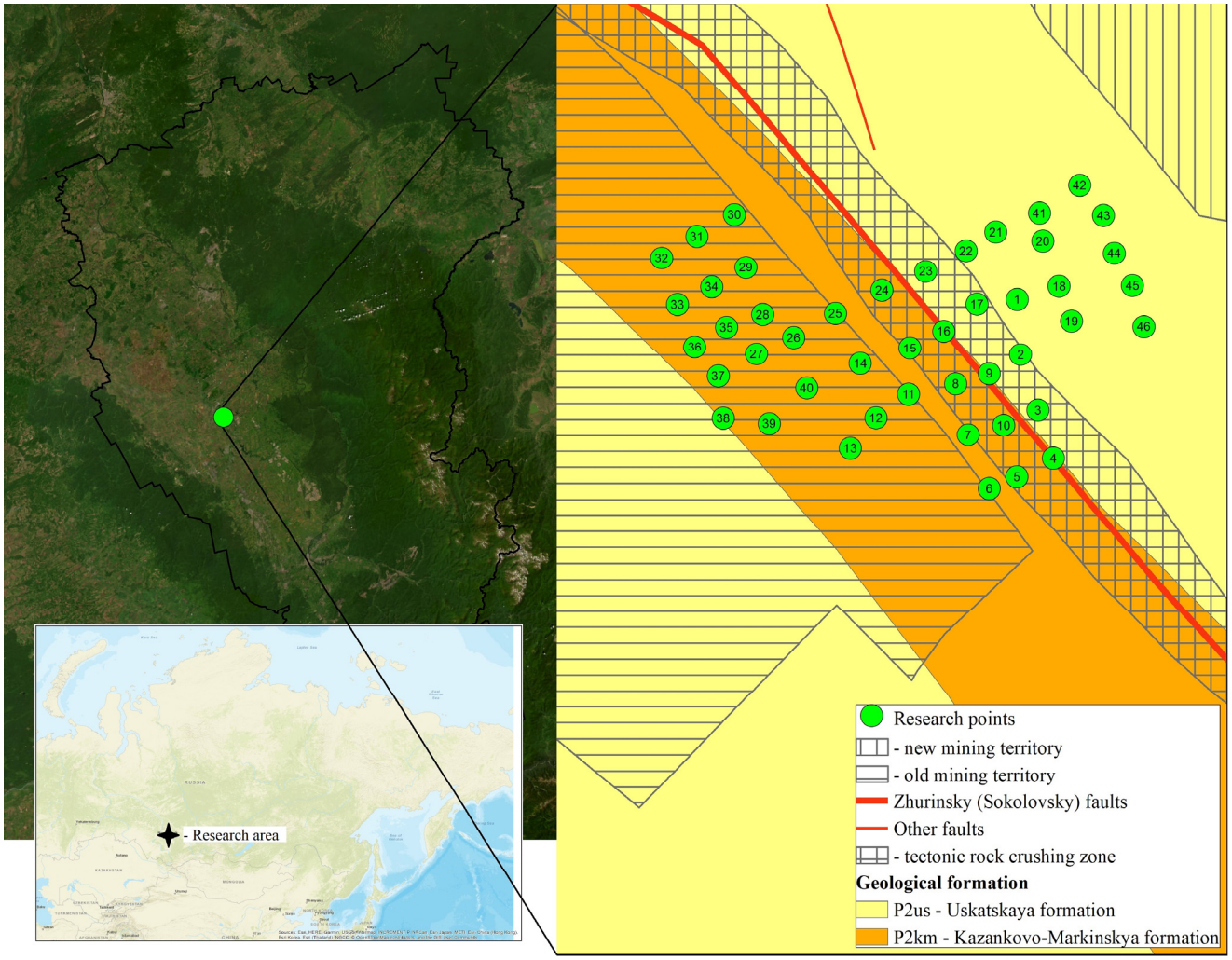


Figure 1. Study area.

The study area comprises two tectonic blocks divided by the Zhurinsky Fault and its disturbance zone. These blocks comprise rocks from the Upper Permian System and are included in the Uskat and Kazankovo–Markinsky formations. These formations are characterized by a rhythmic sequence of sandstones, siltstones, and coals with subordinate mudstones. The Paleozoic rocks have been subject to compression in the form of brachysynclinal folds. Anticlinal folds are of little significance as large interblock faults are typically located along their cores, such as the Zhurinsky and Kilchigizsky Faults, among others. Anticlinal folds are folds in which the rock layers have a convex shape, and the layers dip outward from the axial part toward the periphery.

The Zhurinsky Fault formed as blocks converged and can be associated with strike–slip movements, as well as thrusting in certain areas. This fault corresponds to a significant zone of rock deformation. It is characterized by a change in the displacement incidence angle. The crushing zone thickness, established during prospecting activities, spans up to 300 m [29]. There is an assumption that this disturbance was activated in the Neogene–Quaternary Periods [30].

Permian sediments are overlain by friable deposits of Cretaceous–Paleogene weathering crust and Cenozoic N-Q sediments. The thickness of Quaternary sediments varies between 10 and 60 m and tends to be greater toward watersheds. The following is a description of the most thorough section near the research site. The Miret formation, located at the lowest section, belongs to the Miocene zone of the Neogene Period. Its composition is dense, mottled, montmorillonitic–kaolinitic clay, with rubble, gravel, and carbonate concretions, and with a total thickness of about 7 m. It is overlain by the Mokhov formation belonging to the Pliocene Period of the Neogene System. The thickness of this formation is about 10 m. Its composition is clay with pebbles and gravel, with red-colored fossil soils. Above, the Upper Eopleistocene–Lower Pleistocene deposits are related by genesis to the diluvial–proluvial deposits. This stratum has a thickness of approximately 17.5 m and is primarily made up of clay. Next is the Bachat formation, which belongs to the upper part of the Middle Pleistocene and the lower part of the Upper Pleistocene. The sediment composition genetically refers to the diluvial–proluvial sediments in the form of loams with a total thickness of about 10 m. The alluvial deposits of the second supra-flood terrace (the Krasnobrodskaya formation), located above, belong to the upper section of the Upper Pleistocene. The sediment composition mainly consists of loams with a total thickness of around 24 m. The upper section comprises Upper Pleistocene subaerial deposits, specifically loess-like loams [31].

We evaluated the area around two mines. One mine, designated as “young”, began coal mining in 2018 and is currently active. The second mine in the vicinity of our study area had ceased operations. The effect of distance from these mines on radon content in soil air and its emission was considered separately, as the dynamic processes occurring above these mines may differ in intensity. The potential impact of these factors on the surrounding area may vary accordingly.

The “young” mine is located within the Egozovo–Krasnoyarsk Coal Deposit and corresponds to the syncline of the same name. The mine is characterized by long linear folds oriented parallel to the Salair Ridge. The old mine is located within the Lenin Syncline. In both cases, the rock layers have a concave shape and are inclined toward the axial part of the fold, which is characteristic of synclinal folds. The demarcation between these structures runs along the Zhurinsky Fault. Generally, the intensity of folding and rock disturbance decreases with distance from the main faults, which is, in our case, the Zhurinsky Fault. Disjunctive faults of low amplitude, up to 10 m, have been encountered within both mine areas. These faults could be natural zones of crustal degassing within the mines. Coal in the area has low radioactivity levels, ranging from 1 to 4 μR/h, while coal-bearing rocks exhibit levels of 6–24 μR/h.

2.2. VAR and RFD Measurement

A total of 46 radon measurement points located within 20 points and outside 26 points in the coal minefield were selected to study soil radon concentrations and RFDs.

Soil air probes were collected from 0.6 m-deep wells (80 mm diameter). All wells were drilled at previously selected locations, and the distance between neighboring sample points was 130–190 m. Before measurements, the wells were kept undisturbed for 24 h, covered with a polymer film from above to ensure uniform filling with soil air, and equilibrated between radon and its progeny elements. For soil air sampling, a polyethylene tube (10 mm external diameter) was installed in order to reach the bottom of the well. Inside the tube, there were two silicone tubes (3 mm internal diameter). The air entered the air sampler through one tube and descended into the well through the other, thereby avoiding contamination with outdoor air. Thus, the air was circulated in a closed cycle for 5 min at a rate of 1 l/m using an AV-07 air sampler (NTM-Zaschita, Moscow, Russia). The ascending flow of air passed the cartridge drier and entered the sampling flask. The total sample volume was 50 mL. After each sampling cycle, the system was ventilated with outside air for 2 min. The VAR was measured in a 50 mL air sample tube with an Alfarad+R (NTM-Zaschita, Moscow, Russia) radiometer using an "Air Soil" protocol. This methodology focuses on analyzing the levels of ^{222}Rn, thereby enabling us to determine the concentration of ^{222}Rn in the subterranean atmosphere. The radiometer chamber quantifies the decay of ^{218}Po, which undergoes radioactive decay from ^{222}Rn. Its half-life is 3.05 min. The uncertainty of this monitor is $\pm$30%. This protocol includes corrections for both the standard 50 mL sample tube and the sample collection time. All measurements were performed within 1–8 h of sampling.

RFD was assessed using a "Camera-01" device developed by NTC-NITON in Moscow, Russia. The camera-01 tool assesses the activity of ^{222}Rn by gauging gamma and beta radiation from the short-lived descendants of radon—^{214}Pb and ^{214}Bi—in equilibrium with radon. The accuracy of the device is $\pm$30%. To reach a radon state and its DPR, the chosen sample was left for 4 h after exposure and then examined using a beta sensor. Radon was accumulated through coal sorption columns (SK-13) and a storage chamber (NK-32). Coal in NK-32 chambers adsorbs ^{222}Rn on its surface, providing an estimate of its departure rate from the soil, considering the chamber's known area and sensor installation time. A total of 690 RFD measurements were taken at 46 observation sites. The collection chambers were firmly pressed into the loose soil and then securely sealed after measurements to prevent the release of radon into the atmosphere. At every observation point, 15 cameras were installed. The data from these 15 measurements were averaged, and the resulting values were used for subsequent analysis.

An internal measurement control was carried out for all measurements. The repeated measurements accounted for 15% of the previously conducted measurements. The acquired values complied with the method measurement errors declared by the manufacturer, which was limited to 30%. Radon is typically a mobile phase that varies depending on various factors, such as geological and meteorological conditions, as well as registration methods. A concentration assessment of soil air radon levels with a declared maximum of 30% is adequate to differentiate between hazardous and safe areas, which may differ significantly. More precise measurement techniques are available, such as the use of CR-39 sensors that have a 10% measurement uncertainty. However, they also possess utility constraints. These sensors can assist in enhancing the radon map at a local level in the future. Our study provides primary data on the land near the mines, enabling us to employ existing equipment.

Table 1 shows the location of observation points from areas with a particular determinant.

Table 1. Research points and distance to determining factors.

№	To Old Mining, m	To New Mining, m	To Displacer Fault, m
1	470.7	644.3	249.2
2	357.1	748.8	140.4
3	292.0	835.4	66.2
4	238.0	936.1	2.4
5	104.3	1053.4	129.6
6	8.0	1138.5	224.2
7	57.7	1053.5	163.2
8	133.2	976.7	85.7
9	238.0	869.1	20.6
10	171.0	948.1	52.9
11	0.0	1120.3	227.2
12	0.0	1252.6	359.2
13	0.0	1383.2	490.6
14	0.0	1182.0	283.3
15	100.0	1021.7	125.0
16	220.7	899.1	3.3
17	361.4	758.2	137.6
18	602.7	508.7	383.2
19	556.9	548.2	340.5
20	663.8	457.0	439.5
21	567.7	560.7	339.6
22	453.4	675.9	224.8
23	308.6	821.8	78.8
24	159.0	972.8	72.3
25	0.0	1138.9	238.5
26	0.0	1296.1	395.8
27	0.0	1424.9	524.7
28	0.0	1324.6	424.7
29	0.0	1267.0	367.0
30	0.0	1197.9	283.3
31	0.0	1340.6	423.8
32	0.0	1477.7	559.2
33	0.0	1520.8	618.9
34	0.0	1395.5	494.8
35	0.0	1443.6	543.8
36	0.0	1565.4	665.6
37	0.0	1568.6	668.5
38	0.0	1645.7	745.2
39	0.0	1540.9	641.0
40	0.0	1370.7	470.4
41	716.7	408.8	490.1
42	876.7	247.8	650.7
43	868.9	247.7	646.9
44	812.5	296.8	594.2
45	787.8	320.6	569.9
46	737.8	409.8	511.9

2.3. Statistical Analysis

Data were statistically processed using Statistica 14.0 (StatSoft, Tulsa, OK, USA). Distribution was verified using Kolmogorov–Smirnov, Liliefors, and Shapiro–Wilk tests.

Correlations between RFD, soil radon VAR, and weather conditions were analyzed using the Pearson correlation coefficient.

Fisher's test was employed to examine disparities in both soil radon VAR and RFD among territories (inside/outside mining areas).

Statistical significance was accepted at a $p \leq 0.05$ level.

2.4. Spatial Methods

ArcGIS 10.8.1. software was used for all spatial research methods. To determine the spatial covariance of the data, Moran's I method was employed, with a statistical significance threshold of $p \leq 0.1$. Soil radon and RFD interpolation was performed using the NaturalNeighbor tool in ArcGIS 10.8.1.

2.5. Meteorological Conditions during Research

VAR and RFD were measured on days without precipitation.

Soil radon was measured under similar meteorological conditions, which we present below. The air temperature fluctuated between 11 °C and 21 °C, with an average of 16.39 ± 0.46 °C. The pressure ranged from 978.7 hPa to 989.9 hPa, with an average of 984.2 ± 0.5 hPa. The humidity varied between 43% and 94%, with an average of 65.87 ± 1.92%.

RFD was measured under comparable weather conditions, as detailed below. The air temperature during sorption column exposure ranged from 10.25 °C to 28.6 °C. The mean value was 22.29 ± 0.76 °C. The pressure varied from 968.66 hPa to 985.09 hPa. The mean value was 976.86 ± 0.67 hPa. Air humidity varied from 42.90% to 68.17%. The mean value was 54.13 ± 0.92%.

The temperature, pressure, and humidity met the requirements for conducting measurements according to the specified method, with a margin of error of 30%.

3. Results

3.1. Soil Air VAR

Soil air VAR varied from 3477.7 to 17,520 Bq/m^3 (mean, 9786.9 ± 474.9 Bq/m^3; median, 9383.3 Bq/m^3). These values conform to a normal distribution ($p \leq 0.05$).

No significant correlations were found between soil VAR and distance to radon-determining objects (old or new mine; disturbance displacement), as well as RFD for the entire data set ($p \geq 0.05$).

Soil air VAR outside the mine boundaries varied from 4563.9 to 17,520 Bq/m^3 (mean, 9943.5 ± 618.2 Bq/m^3; median, 9307 Bq/m^3) (Table 2). These values conform to a normal distribution.

Table 2. Descriptive analysis of outside the mine of soil air VAR.

№	Soil Radon VAR, Bq/m^3	SE, Bq/m^3
1	9619.6	2889.1
2	8254.7	2476.0
3	7834.7	2349.3
4	11,650.5	3495.0
5	10,948.3	3283.3
6	11,050.5	3315.0
7	8490.7	2546.7
8	10,562.6	3168.3
9	14,195.2	4261.3
10	10,161.4	3047.1
15	11,717.8	3514.4
16	8559.1	2567.0
17	4563.9	1368.3
18	4937.6	1481.2
19	17,520.0	5254.9
20	8304.5	2490.6
21	16,093.6	4827.2
22	11,789.4	3536.3
23	14,304.8	4291.3
24	8983.1	2693.8
41	6222.4	1866.2

Table 2. *Cont.*

№	Soil Radon VAR, Bq/m^3	SE, Bq/m^3
42	7461.5	2238.1
43	6528.2	1957.6
44	8803.3	2640.0
45	8994.4	2698.1
46	10,978.0	3292.9

No significant correlations were found between VAR in the soil outside the mine boundaries and the distance from the old and new mines, as well as the distance from the displacement of tectonic disturbance. However, a moderate correlation (r = 0.53, $p \leq 0.05$) was found between VAR in soil and the frequency of observation points with RFD values higher than 80 mBq·m^{-2}·s^{-1}.

Soil air VAR within the mine boundary varied from 3477.8 to 15,962.4 Bq/m^3 (mean, 9583.5 ± 755.6 Bq/m^3; median, 9860 Bq/m^3; Table 3). These values conform to a normal distribution.

Table 3. Descriptive analysis of within the mine of soil air VAR.

№	Soil Radon VAR, Bq/m^3	SE, Bq/m^3
11	8892.6	2666.5
12	11,071.2	3320.4
13	3477.8	1043.3
14	8596.5	2578.8
25	6515.8	1953.9
26	9147.1	2743.5
27	10,622.4	3186.0
28	7318.9	2195.1
29	4914.7	1473.7
30	6312.0	1892.7
31	10,572.9	3171.4
32	10,752.3	3225.0
33	13,380.0	4013.1
34	5630.4	1688.4
35	15,962.4	4788.2
36	11,243.1	3372.7
37	7535.0	2260.0
38	14,168.1	4249.6
39	11,013.5	3302.8
40	14,542.5	4361.8

No significant correlations were found between VAR in the soil over the minefield and RFD. Moreover, a moderate correlation was found between VAR in the soil above the mine, the distances of observation points from the new mine (r = 0.46; $p \leq 0.05$), and Zhurinsky Fault displacement (r = 0.46; $p \leq 0.05$).

Table 4 presents the results of the correlation analysis between the VAR and meteorological parameters.

Table 4. Correlations between meteorological data and soil VAR.

	Soil Radon VAR (All Data)	Soil Radon VAR (Outside the Mine)	Soil Radon VAR (Within the Mine)
T, °C	r = 0.40 *	r = 0.61 *	No
P, hPa	No	No	r = 0.46 **
U, %	r = −0.35 **	r = −0.50 *	No

Table 4. *Cont.*

	Soil Radon VAR (All Data)	Soil Radon VAR (Outside the Mine)	Soil Radon VAR (Within the Mine)
T, °C av. 1 h	r = 0.41 *	r = 0.62 *	No
T, °C av. 2 h	r = 0.44 *	r = 0.62 *	No
T, °C av. 3 h	r = 0.44 *	r = 0.61 *	No

* Significance $p \leq 0.01$. ** Significance $p \leq 0.05$.

No significant differences were found between VAR values in soil air over and near the minefield ($p \geq 0.05$).

3.2. RFD

RFD ranged from 10 to 160 mBq·m^{-2}·s^{-1}, with a mean value of 59.76 ± 2.45 mBq·m^{-2}·s^{-1} and a median value of 57.43 mBq·m^{-2}·s^{-1}. The data distribution is normal. In the study area, there were nine monitoring sites with mean values exceeding 80 mBq·m^{-2}·s^{-1}. As per the radiation protection standards (NRB-99/2009) [32] for residential buildings, this necessitates a moderate level of protection against geological radon. At 38 monitoring sites, values above 80 mBq·m^{-2}·s^{-1} were also observed. The percentage of RFD values above 80 mBq·m^{-2}·s^{-1} constituted 0 to 85.7% of all recorded values at each observation point.

We found some correlations between RFD, the distance of the observation points from the mines, and the displacement of the Zhurinsky Fault (Table 5).

Table 5. Correlations between distances to mine and RFD.

	RFD	Median	Max	Min	Interval	Percent over 80
			All data			
Distance to old mine	r = 0.46 *	r = 0.45 *	r = 0.34 **	r = 0.56 *	No	r = 0.49 *
Distance to new mine	r = −0.49 *	r = −0.47 *	r = −0.43 *	r = −0.52 *	No	r = −0.50 *
Distance to displacer fault	No	No	No	r = 0.29 **	r = −0.40 *	No
			Within the mine			
Distance to new mine	r = −0.60 *	r = −0.58 *	r = −0.69 *	r = −0.47 **	r = −0.76 *	r = −0.60 *
Distance to displacer fault	r = −0.58 *	r = −0.56 *	r = −0.67 *	r = −0.44 **	r = −0.75 *	r = −0.58 *
			Outside the mine			
Distance to old mine	r = 0.72 *	r = 0.72 *	r = 0.53 *	r = 0.77 *	No	r = 0.63 *
Distance to new mine	r = −0.73 *	r = −0.72 *	r = −0.53 *	r = −0.77 *	No	r = −0.63 *
Distance to displacer fault	r = 0.70 *	r = 0.69 *	r = 0.45 **	r = 0.80 *	No	r = 0.66 *

* Significance $p \leq 0.01$. ** Significance $p \leq 0.05$.

Table 6 represents the descriptive statistics of outside the mine of RFD.

Table 6. Descriptive analysis of RFD outside the mine.

Research Point	Radon Statistics, mBq·m^{-2}·s^{-1}						
	RFD	SE	Median	Max	Min	Interval	Percent over 80
1	50.27	4.84	53	84	21	63	6.7
2	49.13	5.21	46	83	23	60	0.0
3	34.47	5.04	28	85	12	73	6.7
4	58.53	5.13	55	99	27	72	20.0
5	44.27	4.52	46	69	12	57	0.0
6	39.33	7.28	30	101	10	91	20.0
7	47.73	3.96	43	73	30	43	0.0
8	67.20	5.15	64	95	26	69	33.3
9	54.53	6.51	52	102	10	92	13.3
10	43.53	5.18	44	72	10	62	0.0
15	70.60	3.97	71	98	43	55	26.7

Table 6. *Cont.*

Research Point	Radon Statistics, mBq·m^{-2}·s^{-1}						
	RFD	SE	Median	Max	Min	Interval	Percent over 80
16	65.07	4.52	61	101	41	60	20.0
17	58.87	4.83	59	91	30	61	13.3
18	51.40	8.09	44	144	24	120	13.3
19	81.13	6.01	86	136	47	89	53.3
20	67.67	6.32	67	113	32	81	33.3
21	74.27	7.05	67	124	40	84	33.3
22	73.47	6.15	67	137	35	102	40.0
23	48.87	6.83	42	113	17	96	13.3
24	49.87	6.65	50	86	12	74	20.0
41	64.80	2.63	69	78	46	32	0.0
42	76.93	4.17	77	113	57	56	33.3
43	85.83	4.59	84	115	66	49	66.7
44	87.57	2.45	84.5	115	78	37	85.7
45	83.64	4.15	81.5	116	59	57	71.4
46	82.07	3.77	80.5	108	64	44	50.0

RFD ranged from 10 to 144 mBq·m^{-2}·s^{-1}, with a mean value of 61.96 ± 3.05 mBq·m^{-2}·s^{-1} and a median value of 61.84 mBq·m^{-2}·s^{-1}. The data show a normal distribution. There were nine monitoring sites in the study area with an average value above 80 mBq·m^{-2}·s^{-1}. At 22 monitoring sites, measurements exceeding 80 mBq·m^{-2}·s^{-1} were also detected. The percentage of RFD values above 80 mBq·m^{-2}·s^{-1} measured at each observation point varied between 0% and 85.7%.

Descriptive statistics for the RFD within the mine area are presented in Table 7.

Table 7. Descriptive analysis of RFD within the mine.

Research Point	Radon Statistics, mBq·m^{-2}·s^{-1}						
	RFD	SE	Median	Max	Min	Interval	Percent over 80
11	81.13	7.33	78	160	50	110	40.0
12	86.07	5.87	82	126	55	71	53.3
13	77.53	4.73	77	124	45	79	33.3
14	83.87	6.89	82	137	53	84	53.3
25	60.67	5.22	64	90	29	61	20.0
26	71.20	6.08	68	123	42	81	26.7
27	40.27	5.51	33	80	13	67	6.7
28	56.33	5.23	54	101	25	76	13.3
29	46.33	4.32	44	76	12	64	0.0
30	41.80	5.71	36	83	12	71	6.7
31	52.40	4.82	52	88	19	69	6.7
32	35.00	3.63	38	64	13	51	0.0
33	42.00	3.55	45	60	14	46	0.0
34	68.47	6.46	72	109	34	75	33.3
35	49.40	5.75	50	84	18	66	13.3
36	38.73	4.30	37	74	15	59	0.0
37	37.67	3.51	36	61	18	43	0.0
38	48.00	3.15	46	69	28	41	0.0
39	39.33	3.65	32	62	22	40	0.0
40	81.47	6.26	78	118	43	75	46.7

RFD varied from 12 to 160 mBq·m^{-2}·s^{-1}, with a mean value of 56.88 ± 3.98 mBq·m^{-2}·s^{-1} and a median value of 50.9 mBq·m^{-2}·s^{-1}. Within the study area, four observation locations exhibited a mean value greater than 80 mBq·m^{-2}·s^{-1}. The distribution of the data appears to be normal. Values exceeding 80 mBq·m^{-2}·s^{-1} were recorded at 13 monitoring sites. The

percentage of RFD values above 80 mBq·m^{-2}·s^{-1} measured at each monitoring site varied between 0% and 53.3%.

We found no significant differences between the RFD values at observation points within and near the minefield ($p \geq 0.05$).

We found correlations between the RFD indices and meteorological parameters (Table 8).

Table 8. Correlations between RFD and meteorological parameters.

	Average			Min			Max			Range		
	T	**P**	**U**	**T**	**P**	**U**	**T**	**P**	**U**	**T**	**P**	**U**
						All data						
RFD	No	r = −0.37 *	No	No	r = −0.36 *	No	No	r = −0.36 *	No	No	No	No
Median	No	r = −0.33 **	No	No	r = −0.32 **	No	No	r = −0.31 **	No	No	No	No
Max	r = 0.34 **	r = −0.50 *	No	r = 0.36 *	r = −0.49 *	No	r = 0.37 *	r = −0.50 *	No	No	No	No
Min	No	No	r = 0.30 **	No	No	r = 0.30 **	No	No	No	No	No	No
Interval	r = 0.43 *	r = −0.45 *	No	r = 0.43 *	r = −0.45 *	No	r = 0.46 *	r = −0.46 *	No	r = 0.33 **	No	No
Percent over 80	No	r = −0.33 **	No	No	r = −0.32 **	No	No	r = −0.33 *	No	No	No	No
						Outside the mine						
RFD	No	No	No	No	No	No	No	No	No	No	No	r = −0.39 **
Median	No	No	No	No	No	No	No	No	No	No	No	No
Max	No	No	No	No	No	No	No	No	No	No	No	No
Min	No	No	No	No	No	r = 0.43 **	No	No	No	No	No	r = −0.42 **
Interval	No	No	No	No	No	No	No	No	No	r = 0.47 **	No	No
Percent over 80	No	No	No	No	No	No	No	No	No	No	No	r = −0.43 **
						Within the mine						
RFD	r = 0.91 *	r = −0.92 *	No	r = 0.91 *	r = −0.92 *	No	r = 0.91 *	r = −0.92 *	No	No	r = 0.67 *	No
Median	r = 0.88 *	r = −0.88 *	No	r = 0.88 *	r = −0.88 *	No	r = 0.88 *	r = −0.88 *	No	No	r = 0.63 *	No
Max	r = 0.90 *	r = −0.88 *	No	r = 0.91 *	r = −0.88 *	No	r = 0.89 *	r = −0.88 *	No	No	r = 0.66 *	No
Min	r = 0.88 *	r = −0.89 *	No	r = 0.85 *	r = −0.88 *	No	r = 0.88 *	r = −0.88 *	No	No	r = 0.75 *	No
Interval	r = 0.75 *	r = −0.71 *	No	r = 0.79 *	r = −0.72 *	No	r = 0.74 *	r = −0.73 *	No	No	r = 0.46 **	No
Percent over 80	r = 0.93 *	r = −0.95 *	No	r = 0.92 *	r = −0.94 *	No	r = 0.94 *	r = −0.94 *	No	No	r = 0.64 *	No

* Significance $p \leq 0.01$. ** Significance $p \leq 0.05$.

3.3. Spatial Patterns of RFD and Soil Air VAR

Table 9 displays the spatial data of Moran's I autocorrelation. A significant clustering of data was found for RFD. Such a conclusion cannot be made for soil VAR values, which exhibit chaotic spatial distribution.

Table 9. Descriptive analysis of Moran's I.

	All Measurements		**Within Mine**		**Outside Mine**	
	Soil Air VAR	**RFD**	**Soil Air VAR**	**RFD**	**Soil Air VAR**	**RFD**
Observed	−0.093866	0.574609	0.001870	0.380507	−0.085938	0.748294
Expected	−0.022222	−0.022222	−0.052632	−0.052632	−0.040000	−0.040000
Standard Deviation	0.018784	0.019254	0.029452	0.030485	0.046699	0.049477
z-score	−0.522736	4.301207	0.317583	2.480769	−0.212578	3.543949
p-value	0.601158	0.000017	0.750802	0.013110	0.831656	0.000394

Figure 2 shows the characteristics of the spatial variation in soil radon VAR and RFD within the study area.

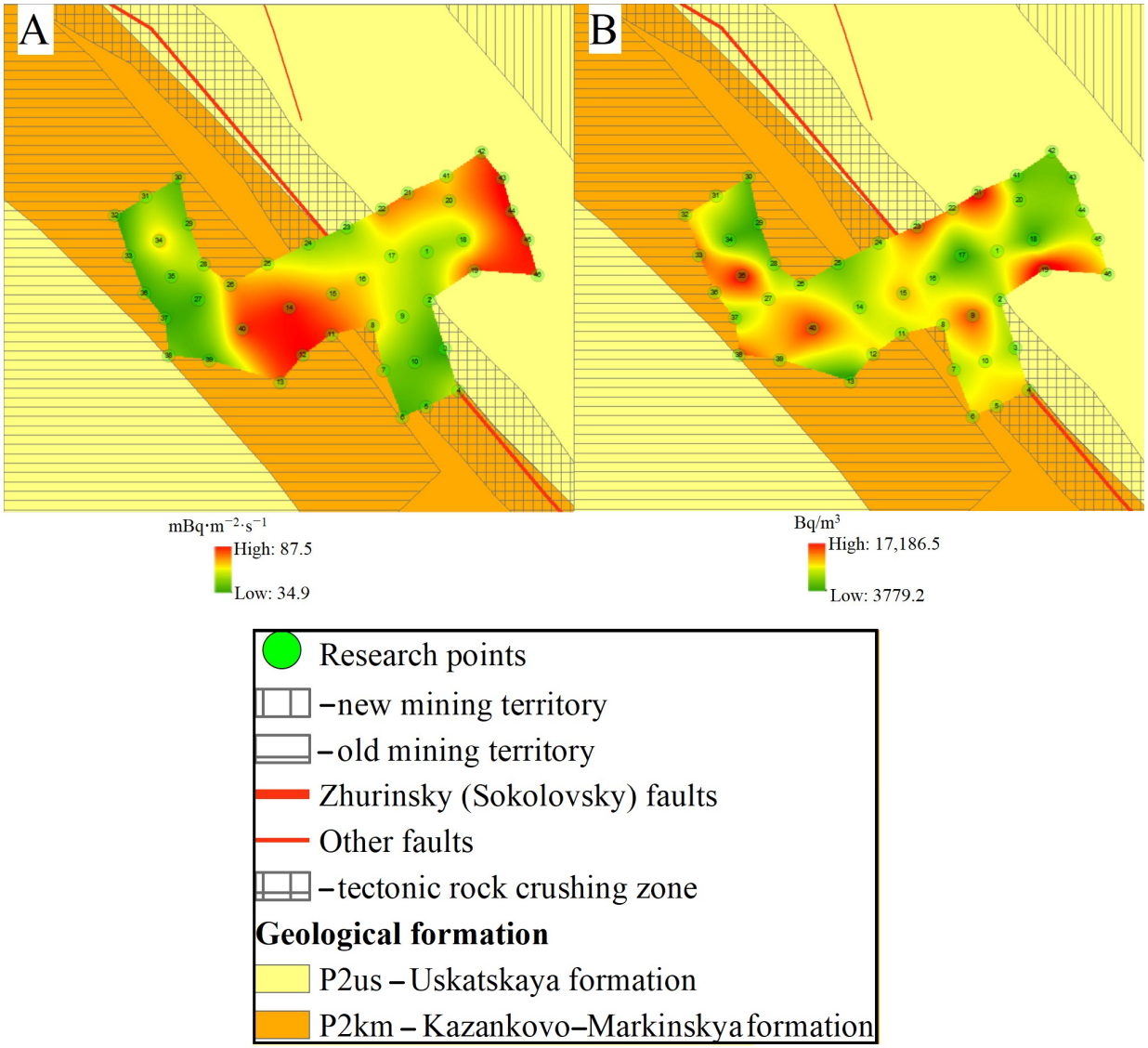


Figure 2. Spatial features of RFD (**A**) and soil VAR (**B**).

4. Discussion

4.1. VAR in Soil Air

High average soil air VAR for the studied coal field implies the presence of two main factors acting separately or together: (1) a high content of uranium, thorium, and radium in the upper soil horizon; (2) the presence of a permeable zone for radon release from deeper horizons. Insufficient data are available to support the first factor. No anomalies were detected during previous exploration works at this site, and measurements of the gamma field with the radiometer (SRP-68-01) did not detect any anomalies either. The permeable zone, even with low concentrations of radon parent elements, will still transport a large amount of radon to the surface through diffusion–convection transport. Part of the examined area belongs to the mining area, another area was affected by disjunctive disturbance, and some measurements were made in the area outside these conditions. However, we did not notice any significant differences in soil radon levels between these locations.

The absence of significant correlations between soil radon and the distance to the disturbance as well as to the mine indicates that our study area is probably entirely within the zone of influence of these factors, given the significant increase in soil VAR for such depths. However, this statement needs to be verified by studying a control area far away

from the mines. It is additionally affirmed by the lack of statistically significant variations between the mean values of soil radon inside and outside the mine area.

These findings have been attributed to certain hypotheses. As previously mentioned, tectonic disturbances lead to zones of rock crushing, which allows for radon emanation [33,34]. The primary factors responsible for the manifestation of gas anomalies of this nature have been recognized as fault dynamics (i.e., fault activity) and types (i.e., dynamic types, such as thrusting, faulting, and fault rupture, among others), as well as other factors [35–37]. Additionally, the unusual concentration of soil radon within the zone of disturbance and its crushing area is more extensive [16,38]. Furthermore, it is plausible that the augmented release of radon through faults stems from the concentration of radioactive substances within the fault [39,40].

Another factor to consider is underground coal mining. The mining process causes the collapse of the above-mine space. Even minor alterations to the stress–strain state result in modifying the radon field in the geological surroundings [41,42]. Radon anomalies can facilitate the detection, in some cases, of erratically situated subterranean activities, which are distinctive of the initial phases of coal deposit formation [43]. Such findings are rather prevalent throughout the study area. Linear anomalies of radon gas release were previously observed along the worked-out longwall face and can be assumed to occur throughout the entire minefield. The stretching zone, in this case, may extend beyond the boundaries of the working area and the minefield. Based on field observations of the mine space and natural stretching structures, such as grabens and dumps, the stretching zones exhibit good permeability for deep gases [18,23]. Similar to our study, remarkably elevated levels of soil radon were recorded in the Upper Silesian Basin, albeit from slightly deeper boreholes [23]. In areas where coal mining has taken place, the migration of gases from the mine continues uncontrollably and chaotically even after the end of the mining process [44]. These gases include methane, carbon dioxide, and radon.

The effect of mining on the growth of soil VAR may not be related to the geodynamics of the space above the mine and the creation of zones of increased permeability. Radon can be transported directly from the mine through the natural fault zone to the surface, thus significantly enriching the soil with radon compared to other soil gases. Coal mines can accumulate significantly high concentrations of radon in the air, especially in dead-end and collapsed areas after mining [45,46]. This mechanism has been proposed in studies by Miklyaev P.S. et al. [44,47,48]. This phenomenon can occur when coal is mined up to the fracture zone of fault rocks (most often, large faults are the natural boundaries of the mine and the coal deposits). In our study, we examined the area surrounding the Zhurinsky Fault, which acts as the boundary for coal mining. Radon can be transported from the mine through this fault, as well as the crushing zones formed as a consequence of mining activities. In previous research, we acquired elevated volumetric radon activity measurements within residential buildings near the East Kamyshan Fault, situated within the mine area. Specifically, in one of the buildings, in close proximity to this radon source, the radon concentration in the basement reached 20,000 Bq/m^3 during the summer, when the "pump" effect of soil radon into the room was reduced. Furthermore, the RFD was significantly greater than in other monitored areas [21].

To confirm the presence of radon removal from the tectonic disturbance zone rather than the mine, it is necessary to analyze the gas composition of the soil above the disturbance zone. If free hydrogen (H2) is present, it can be concluded that removal is occurring from deep horizons in the Earth's crust along the fault zone, rather than from the mine. The simultaneous presence of high levels of methane, hydrogen, and radon may indicate that radon has migrated from deeper horizons, which is possible in the presence of a permeable medium that is characteristic of faults. Conversely, low levels of methane and hydrogen in combination with high levels of radon suggest radon formation through the decay of radium within near-surface geological conditions.

The stimulation of radon emission to the surface can occur due to coal-bearing strata gases, such as methane, carbon dioxide, etc., under both mine and fault influences [49–51].

Any of the described possibilities will make it possible to predict hazards in the surrounding areas of mines. The obtained soil radon levels are significantly high, which may result in the migration of similar levels of radon into residential buildings. As is widely acknowledged, there is a strong correlation between the concentration of radon in soil air and radon levels found in residential buildings [52,53]. Previously, we detected significant levels of radon in residential structures situated on the periphery of a coal mine. The highest recorded VAR values reached 1705 Bq/m^3, and approximately 21% of residential buildings had values above 200 Bq/m^3. High VAR levels were also detected in dwellings located within 1 km of the Zhurinsky Fault, with a mean value of 331.9 Bq/m^3 [21,22,54]. Coal and coal-bearing rocks can contain high concentrations of uranium and radium, which also affect the radon content in mine workings and faults crossing coal layers [55,56].

According to the Swedish Radon Criteria [57], if soil radon content is below 10,000 Bq/m^3, no further measures are needed during residential building construction. For values between 10,000 Bq/m^3 and 50,000 Bq/m^3, additional measures are required to decrease indoor radon levels. For levels above 50,000 Bq/m^3, increased protective action is necessary during construction. About 48% of the studied surveyed areas are within these criteria. However, it should be noted that the level of risk is both positively correlated with the permeability of the topsoil layer and influenced by local conditions [58]. This figure may fluctuate in either direction.

The moderate correlation between meteorological conditions (air temperature and humidity) and soil radon confirms the connection between the upper lithospheric air and the atmosphere moving via convection, diffusion, and other forces [59–61]. In wells of selected depths, an atmosphere–soil–air connection is expected, and air temperature is an important factor in radon release into the atmosphere [62–64], especially in permeable fault environments [65,66]. This is supported by the increased correlation between the soil and the atmosphere outside the mine. Radon concentrations typically increase as depth increases and become less sensitive to meteorological parameters [67]. Therefore, using soil radon data from deep horizons to predict RFD is not recommended.

4.2. RFD

No correlation was found between soil VAR and RFD in any of the compared cases. In this study, we only discovered a correlation between radon concentration in soil and the frequency of observation points with high RFD (over 80 mBq·m^{-2}·s^{-1}) in the location outside the mine ($r = 0.53$, $p \leq 0.05$). This finding suggests that an increase in radon concentration in soil does not necessarily result in an increase in RFD, but it increases the chance of encountering high values. Similar results were previously obtained in loose rocks of a similar composition [68,69]. It is known that the relationship between RFD and soil radon decreases as depth increases. Additionally, there are cases where RFD can decrease in clay soils, despite an increase in soil radon due to a reduction in its release rate into the atmosphere [70]. Therefore, when evaluating the risk of radon in a region, it is important to consider the presence of high radon levels in soil.

A strong correlation between RFD and thermal–barometric conditions in the atmosphere was found. The occurrence of air temperature differences between the soil and the surface layer of the atmosphere leads to an increase in RFD due to the "pump" effect [24,25]. Humidity is also known to be closely related to radon emission [71]. The lack of a relationship between humidity and radon concentrations in the atmosphere may be caused by a small temperature difference in a larger number of observations. This results in the humidity not reaching the dew point, thus preventing condensation on the soil surface. Consequently, this does not affect radon emanation from the soil during morning measurements.

The obtained RFD values have a rather high level compared to previous studies [54]. However, the values obtained when estimating the RFD above the minefield were much higher, at 181.59 ± 13.32 mBq·m^{-2}·s^{-1} [21]. In addition, the values in areas outside the mines (33.07 ± 1.78 mBq·m^{-2}·s^{-1}) and the tectonic disturbance areas were significant. Areas with comparable RFD levels were found inside the minefield in both our previous work [21] and similar studies [23]. Thus, we can conclude that the minefield is not com-

pletely dangerous in terms of radon emanation, only if there are permeable zones and the composition of the surface layer is suitable. In general, the obtained results indicate that it is necessary to introduce anti-radon measures in all studied areas, provided a decision is made to develop this territory.

The observed correlation between the distance from the minefield and the RFD may be evidence of the formation of zones with increased radon permeability in the vicinity of mines, especially old mines, and tectonic disturbance zones. Regarding the mine area, changes in radiological indicators can occur continuously and for quite a long time, even after the closure of the mine [27]. This suggests that decisions on the radon safety of geological environments may change over time and that mandatory monitoring is required.

Figure 2 also shows the lack of a relationship between the RFD and VAR of soil air. Soil radon is characterized by spotty- or halo-shaped anomalies, although the values obtained are generally very high and similar in most measurements. RFD is also characterized by spotty-shaped anomalies, but it is offset relative to the soil VAR anomalies. The high clustering of the RFD data indicates similar conditions for radon emanations in different parts of the study area. For radon anomalies, the presented forms of anomalies are typical [72–74], and in our case, it is better to discuss the homogeneity of values for the whole study area, taking into account the measurement errors of the instrument. The most probable is that all the observation points are located within the areas of influence of the Zhurinsky Fault or the mining area.

5. Conclusions

In this study, the concentration of soil radon and its emanation to the surface were studied at the edge of a minefield, as well as areas within its vicinity. No significant correlation was found between soil VAR and RFD. The high radon concentrations in the soils of this area present a radiological hazard to the residential population, especially those with houses with underground levels. The high level of radon emanation makes it necessary to design high-quality ventilation systems in new and existing houses. The meteorological parameters, such as air temperature, pressure, and humidity, were correlated with RFD and VAR. In permeable rock zones, the importance of radon convection from deep layers of the Earth's crust increases, thus highlighting the significance of considering meteorological parameters. Special attention should be paid to underground coal mining areas and their surroundings in coal mining regions around the world. The regions over mines are radiologically dangerous areas due to the presence of radon-permeable zones created via the collapse of mine workings. The disturbance zone, which is often the boundary of coal deposits, can also have a high radiological impact. Radon flows through this area is facilitated via convection–diffusion. The source of radon may not only be exclusively from the disentangled rocks of the tectonic disturbance zone but could also come from mine workings. Air entering the weakened disturbance zone from the mine workings is a potential source of indoor radon that needs to be verified through field studies. The obtained values of radon concentration in soils and RFD allow us to conclude that this marginal part of the mine and its surroundings are at risk from radon.

Currently, there is a lack of long-term observation monitoring or extensive preliminary studies into the radon hazard of soils near mine workings, including disturbance zones. These findings should be used to create temporary recommendations for the population to decrease exposure to radon until hazardous zones are identified and delineated. The primary approach to safeguarding homes in these regions uses forced ventilation of subterranean areas or their separation from primary residential zones. Additionally, increasing room ventilation is a crucial temporary measure, despite its limited effectiveness in the challenging winter climate of the research location. In the future, a key necessity for these regions is the establishment of a monitoring network aimed at assessing the characteristics of the radon field.

Author Contributions: Conceptualization, T.L. and A.L.; methodology, T.L.; software, T.L.; validation, K.L., T.L. and A.L.; formal analysis, T.L. and A.L.; investigation, K.L., T.L. and A.L.; resources, T.L. and A.L.; data curation, T.L.; writing—original draft preparation, T.L. and A.L.; writing—review and editing, K.L., T.L. and A.L.; visualization, T.L.; supervision, T.L.; project administration, A.L.; funding acquisition, A.L. All authors have read and agreed to the published version of the manuscript.

Funding: This research was funded by the Russian Science Foundation (RSF) under research project № 23-27-00320, https://rscf.ru/en/project/23-27-00320/ (accessed on 31 October 2023).

Institutional Review Board Statement: Not applicable.

Informed Consent Statement: Not applicable.

Data Availability Statement: The data presented in this study are available in article.

Conflicts of Interest: The authors declare no conflict of interest.

References

1. Bhaskaran, R.; Damodaran, R.C.; Kumar, V.A.; Panakal John, J.; Bangaru, D.; Natarajan, C.; Sathiamurthy, B.S.; Mundiyanikal Thomas, J.; Mishra, R. Inhalation Dose and Source Term Studies in a Tribal Area of Wayanad, Kerala, India. *J. Environ. Public Health* **2017**, *2017*, e1930787. [CrossRef] [PubMed]
2. Kang, J.K.; Seo, S.; Jin, Y.W. Health Effects of Radon Exposure. *Yonsei Med. J.* **2019**, *60*, 597–603. [CrossRef] [PubMed]
3. Georgakilas, A.G.; O'Neill, P.; Stewart, R.D. Induction and Repair of Clustered DNA Lesions: What Do We Know so Far? *Radiat. Res.* **2013**, *180*, 100–109. [CrossRef]
4. Reddy, A.; Conde, C.; Peterson, C.; Nugent, K. Residential Radon Exposure and Cancer. *Oncol. Rev.* **2022**, *16*, 558. [CrossRef] [PubMed]
5. Radon. Available online: https://www.who.int/news-room/fact-sheets/detail/radon-and-health (accessed on 23 October 2023).
6. Ma, Y.; Bringemeier, D.; Scheuermann, A.; Molebatsi, T.; Li, L. Fault and fracture zone detection based on soil gas mapping and gamma ray survey at the extension site of an open pit coal mine. In Proceedings of the 12th Coal Operators' Conference, Wollongong, Australia, 16–17 February 2012.
7. Giustini, F.; Ruggiero, L.; Sciarra, A.; Beaubien, S.E.; Graziani, S.; Galli, G.; Pizzino, L.; Tartarello, M.C.; Lucchetti, C.; Sirianni, P.; et al. Radon Hazard in Central Italy: Comparison among Areas with Different Geogenic Radon Potential. *Int. J. Environ. Res. Public Health* **2022**, *19*, 666. [CrossRef]
8. Wang, N.; Yang, J.; Wang, H.; Jia, B.; Peng, A. Characteristics of Indoor and Soil Gas Radon, and Discussion on High Radon Potential in Urumqi, Xinjiang, NW China. *Atmosphere* **2023**, *14*, 1548. [CrossRef]
9. Borgoni, R.; Tritto, V.; Bigliotto, C.; De Bartolo, D. A Geostatistical Approach to Assess the Spatial Association between Indoor Radon Concentration, Geological Features and Building Characteristics: The Case of Lombardy, Northern Italy. *Int. J. Environ. Res. Public Health* **2011**, *8*, 1420–1440. [CrossRef]
10. Gavriliev, S.; Petrova, T.; Miklyaev, P.; Karfidova, E. Predicting Radon Flux Density from Soil Surface Using Machine Learning and GIS Data. *Sci. Total Environ.* **2023**, *903*, 166348. [CrossRef]
11. Tsvetkova, T.; Przylibski, T.A.; Nevinsky, I.; Nevinsky, V. Measurement of Radon in the East Europe under the Ground. *Radiat. Meas.* **2005**, *40*, 98–105. [CrossRef]
12. Cinelli, G.; Tositti, L.; Capaccioni, B.; Brattich, E.; Mostacci, D. Soil Gas Radon Assessment and Development of a Radon Risk Map in Bolsena, Central Italy. *Environ. Geochem. Health* **2015**, *37*, 305–319. [CrossRef]
13. Kemski, J.; Klingel, R.; Siehl, A.; Valdivia-Manchego, M. From Radon Hazard to Risk Prediction-Based on Geological Maps, Soil Gas and Indoor Measurements in Germany. *Environ. Geol.* **2009**, *56*, 1269–1279. [CrossRef]
14. Moussa, M.M.; El Arabi, A.-G.M. Soil Radon Survey for Tracing Active Fault: A Case Study along Qena-Safaga Road, Eastern Desert, Egypt. *Radiat. Meas.* **2003**, *37*, 211–216. [CrossRef]
15. Utkin, V.I.; Yurkov, A.K. Radon as a Tracer of Tectonic Movements. *Russ. Geol. Geophys.* **2010**, *51*, 220–227. [CrossRef]
16. Seminsky, K.Z.; Bobrov, A.A. Radon Activity of Faults (Western Baikal and Southern Angara Areas). *Russ. Geol. Geophys.* **2009**, *50*, 682–692. [CrossRef]
17. Ball, T.K.; Wysocka, M. Radon in Coalfields in the United Kingdom and Poland. *Arch. Min. Sci.* **2011**, *56*, 249–264.
18. Klingel, R.; Kemski, J. Influence of Underground Mining on the Geogenic Radon Potential. *Radon Living Environ.* **1999**, 773–786.
19. Palchik, V. Localization of Mining-Induced Horizontal Fractures along Rock Layer Interfaces in Overburden: Field Measurements and Prediction. *Environ. Geol.* **2005**, *48*, 68–80. [CrossRef]
20. Wysocka, M.; Chalupnik, S. Correlation of Radon Concentration Level with Mining and Geological Conditions in Upper Silesia Region. *J. Min. Sci.* **2003**, *2*, 199–206. [CrossRef]
21. Leshukov, T.; Larionov, A.; Legoshchin, K.; Lesin, Y.; Yakovleva, S. The Assessment of Radon Emissions as Results of the Soil Technogenic Disturbance. *Int. J. Environ. Res. Public Health* **2020**, *17*, 9268. [CrossRef]
22. Leshukov, T.; Larionov, A.; Legoshchin, K.; Yakovleva, S. Radon Hazard Assessment in Region with Intense Coal Mining Industry. *IOP Conf. Ser. Earth Environ. Sci.* **2020**, *543*, 012026. [CrossRef]

23. Wysocka, M.; Skubacz, K.; Chmielewska, I.; Urban, P.; Bonczyk, M. Radon Migration in the Area around the Coal Mine during Closing Process. *Int. J. Coal Geol.* **2019**, *212*, 103253. [CrossRef]
24. Schery, S.D.; Gaeddert, D.H. Measurements of the Effect of Cyclic Atmospheric Pressure Variation on the Flux of 222RN from the Soil. *Geophys. Res. Lett.* **1982**, *9*, 835–838. [CrossRef]
25. Modibo, O.B.; Tamakuma, Y.; Suzuki, T.; Yamada, R.; Zhuo, W.; Kranrod, C.; Iwaoka, K.; Akata, N.; Hosoda, M.; Tokonami, S. Long-Term Measurements of Radon and Thoron Exhalation Rates from the Ground Using the Vertical Distributions of Their Activity Concentrations. *Int. J. Environ. Res. Public Health* **2021**, *18*, 1489. [CrossRef] [PubMed]
26. Lu, W.; Cao, Y.-J.; Tien, J. Method for Prevention and Control of Spontaneous Combustion of Coal Seam and Its Application in Mining Field. *Int. J. Min. Sci. Technol.* **2017**, *27*, 839–846. [CrossRef]
27. Wysocka, M.; Nowak, S.; Chałupnik, S.; Bonczyk, M. Radon Concentrations in Dwellings in the Mining Area—Are There Observed Effects of the Coal Mine Closure? *Int. J. Environ. Res. Public Health* **2022**, *19*, 5214. [CrossRef] [PubMed]
28. Adushkin, V.V. Technogenic tectonic seismicity in Kuzbass. *GiG* **2018**, *59*, 709–724. [CrossRef]
29. Lavrenov, P.F.; Snegko, B.A.; Shigrev, A.F.; Shelemeteva, A.V.; Filippova, N.V. *State Geological Map of the Russian Federation. Scale 1: 200,000*, 2nd ed.; Kuzbass Series. Sheet N-45-XV (Leninsk-Kuznetsky). Explanatory Letter; VSEGEI: Moscow, Russia, 2018.
30. Novikov, I.S.; Cherkas, O.V.; Mamedov, G.M.; Simonov, Y.G.; Simonova, T.Y.; Nastavko, V.G. Activity stages and tectonic division in the Kuznetsk Basin, Southern Siberia. *Russ. Geol. Geophys.* **2013**, *54*, 324–334. [CrossRef]
31. Bichkov, A.I.; Shatilova, G.I.; Shigrev, A.F. *Geological Structure and Minerals of the Central Part of Kuzbass. Report of the Kuzbass Party on the Compilation of a Geological Map and a Map of Mineral Resources at a Scale of 1:50,000 on the Gramoteinskaya Area within the Framework of Sheets No. 45-41-B, D and No. 45-53-A, B, C, G*; KPR Kemerovskoy Oblasti: Novokuznetsk, Russia, 1998.
32. *NRB99/2009*; Radiation Safety Standards: Sanitary and Epidemiological Rules and Regulations. Federal Center for Hygiene and Epidemiology of Rospotrebnadzor: Moscow, Russia, 2009.
33. Neri, M.; Giammanco, S.; Leonardi, A. Preliminary Indoor Radon Measurements Near Faults Crossing Urban Areas of Mt. Etna Volcano (Italy). *Front. Public Health* **2019**, *7*, 105. [CrossRef] [PubMed]
34. Benà, E.; Ciotoli, G.; Ruggiero, L.; Coletti, C.; Bossew, P.; Massironi, M.; Mazzoli, C.; Mair, V.; Morelli, C.; Galgaro, A.; et al. Evaluation of tectonically enhanced radon in fault zones by quantification of the radon activity index. *Sci. Rep.* **2022**, *12*, 21586. [CrossRef]
35. Annunziatellis, A.; Beaubien, S.E.; Bigi, S.; Ciotoli, G.; Coltella, M.; Lombardi, S. Gas Migration along Fault Systems and through the Vadose Zone in the Latera Caldera (Central Italy): Implications for CO_2 Geological Storage. *Int. J. Greenh. Gas Control* **2008**, *2*, 353–372. [CrossRef]
36. Seminsky, K.; Bobrov, A.A.; Sodnomsambuu, D. Radon and Tectonic Activity of the Faults at the Central Mongolia. *Dokl. Akad. Nauk* **2019**, *487*, 538–542. [CrossRef]
37. Seminskii, K.; Bobrov, A.A.; Sodnomsambuu, D. Relationship between Radon and the Tectonic Activity of Faults in Central Mongolia. *Dokl. Earth Sci.* **2019**, *487*, 890–893. [CrossRef]
38. Seminsky, K.Z.; Bobrov, A.A.; Demberel, S. Variations in radon activity in the crustal fault zonez: Spatial characteristics. *Izvestiya. Phys. Solid Earth* **2014**, *50*, 795–813. [CrossRef]
39. Pereira, A.J.S.C.; Neves, L.J.P.F. Estimation of the Radiological Background and Dose Assessment in Areas with Naturally Occurring Uranium Geochemical Anomalies—A Case Study in the Iberian Massif (Central Portugal). *J. Environ. Radioact.* **2012**, *112*, 96–107. [CrossRef] [PubMed]
40. Cho, S.Y.; Koo, M.-H.; Cho, B.W.; Jung, Y.-Y.; Oh, Y.H. Factors Controlling the Spatial and Temporal Variability in Groundwater 222Rn and U Levels. *Water* **2019**, *11*, 1796. [CrossRef]
41. Galiana-Merino, J.J.; Molina, S.; Kharazian, A.; Toader, V.-E.; Moldovan, I.-A.; Gómez, I. Analysis of Radon Measurements in Relation to Daily Seismic Activity Rates in the Vrancea Region, Romania. *Sensors* **2022**, *22*, 4160. [CrossRef] [PubMed]
42. Kozlova, I.A.; Yurkov, A.K.; Biryulin, S.V. Variations in the volume activity of radon during technogenic and tectonic seismic events. *GIAB* **2022**, 119–130. [CrossRef]
43. Long, J.; Liu, J.; Zhang, S.; Li, M. Comprehensive Evaluation of Goaf Range in a Coal Mine with a Complex Terrain through CSAMT and an Activated-Carbon Method for Radon Measurement. *Appl. Sci.* **2023**, *13*, 4274. [CrossRef]
44. Chećko, J.; Howaniec, N.; Paradowski, K.; Smolinski, A. Gas Migration in the Aspect of Safety in the Areas of Mines Selected for Closure. *Resources* **2021**, *10*, 73. [CrossRef]
45. Zhou, B.; Chang, P.; Xu, G. Computational Fluid Dynamic Simulation of Inhaled Radon Dilution by Auxiliary Ventilation in a Stone-Coal Mine Laneway and Dosage Assessment of Miners. *Processes* **2019**, *7*, 515. [CrossRef]
46. Fijałkowska–Lichwa, L.; Przylibski, T.A. Radon (222Rn) as a Tracer in Natural Ventilation Efficiency Assessment in Underground Workings—An Example of „St John Mine" Tourist Complex in Krobica (the Sudetes, SW Poland). *J. Environ. Radioact.* **2023**, *265*, 107225. [CrossRef]
47. Asimakou, K.; Kallithrakas-Kontos, N.; Vafeidis, A.; Manoutsoglou, E. Distribution of Radon Concentrations in Active and Inactive Underground Mines: A Literature Review. *Mater. Proc.* **2021**, *5*, 38. [CrossRef]
48. Peter, M.; Tat'yana, P.; Dmitry, S.; Pavel, S.; Tsebro, D.N. Dynamics of Radon Emission from the Adits of the Former Uranium Mine on the Mount Beshtau. *ANRI* **2022**, 44–60. [CrossRef]
49. Etiope, G.; Lombardi, S. Evidence for Radon Transport by Carrier Gas through Faulted Clays in Italy. *J. Radioanal. Nucl. Chem.* **1995**, *193*, 291–300. [CrossRef]

50. Cvetković, M.; Kapuralić, J.; Pejić, M.; Kolenković Močilac, I.; Rukavina, D.; Smirčić, D.; Kamenski, A.; Matoš, B.; Špelić, M. Soil Gas Measurements of Radon, CO_2 and Hydrocarbon Concentrations as Indicators of Subsurface Hydrocarbon Accumulation and Hydrocarbon Seepage. *Sustainability* **2021**, *13*, 3840. [CrossRef]
51. Dyck, W.; Jonasson, I.R. Chapter 11 Radon. In *Handbook of Exploration Geochemistry*; Hale, M., Ed.; Geochemical Remote Sensing of the Sub-Surface; Elsevier Science B.V.: Amsterdam, The Netherlands, 2000; Volume 7, pp. 353–394.
52. Chen, J.; Falcomer, R.; Bergman, L.; Wierdsma, J.; Ly, J. Correlation of Soil Radon and Permeability with Indoor Radon Potential in Ottawa. *Radiat. Prot. Dosim.* **2009**, *136*, 56–60. [CrossRef] [PubMed]
53. Esan, D.T.; Sridhar, M.K.C.; Obed, R.; Ajiboye, Y.; Afolabi, O.; Olubodun, B.; Oni, O.M. Determination of Residential Soil Gas Radon Risk Indices Over the Lithological Units of a Southwestern Nigeria University. *Sci. Rep.* **2020**, *10*, 7368. [CrossRef] [PubMed]
54. Leshukov, T. Radon Hazard in Underground Coal Mining Areas (Using the Example of the Kuznetsk Coal Basin). Ph.D. Thesis, KemSU, Grozny, Russia, 2021.
55. Okeme, I.C.; Scott, T.B.; Martin, P.G.; Satou, Y.; Ojonimi, T.I.; Olaluwoye, M.O. Assessment of the Mode of Occurrence and Radiological Impact of Radionuclides in Nigerian Coal and Resultant Post-Combustion Coal Ash Using Scanning Electron Microscopy and Gamma-Ray Spectroscopy. *Minerals* **2020**, *10*, 241. [CrossRef]
56. Transbaikal State University; Sidorova, G.P.; Krylov, D.A.; National Research Centre "Kurchatov Institute". Radiation hazard issues in the coal power generation industry. *MIAB* **2017**, *11*, 200–209. [CrossRef]
57. Lara, E.; Rocha, Z.; Palmieri, H.E.L.; Santos, T.O.; Rios, F.J.; Oliveira, A.H. Radon Concentration in Soil Gas and Its Correlations with Pedologies, Permeabilities and 226Ra Content in the Soil of the Metropolitan Region of Belo Horizonte—RMBH, Brazil. *Radiat. Phys. Chem.* **2015**, *116*, 317–320. [CrossRef]
58. Nunes, L.J.R.; Curado, A.; Lopes, S.I. The Relationship between Radon and Geology: Sources, Transport and Indoor Accumulation. *Appl. Sci.* **2023**, *13*, 7460. [CrossRef]
59. Smetanová, I.; Holý, K.; Müllerová, M.; Polášková, A. The Effect of Meteorological Parameters on Radon Concentration in Borehole Air and Water. *J. Radioanal. Nucl. Chem.* **2010**, *283*, 101–109. [CrossRef]
60. Hinkle, M.E. Environmental Conditions Affecting Concentrations of He, CO_2, O_2 and N_2 in Soil Gases. *Appl. Geochem.* **1994**, *9*, 53–63. [CrossRef]
61. Szabó, K.Z.; Jordan, G.; Horváth, Á.; Szabó, C. Dynamics of soil gas radon concentration in a highly permeable soil based on a long-term high temporal resolution observation series. *J. Environ. Radioact.* **2013**, *124*, 74–83. [CrossRef]
62. Haquin, G.; Zafrir, H.; Ilzycer, D.; Weisbrod, N. Effect of Atmospheric Temperature on Underground Radon: A Laboratory Experiment. *J. Environ. Radioact.* **2022**, *253–254*, 106992. [CrossRef]
63. Catalano, R.; Immé, G.; Mangano, G.; Morelli, D.; Aranzulla, M. Radon Transport: Laboratory and Model Study. *Radiat. Prot. Dosim.* **2015**, *164*, 575–581. [CrossRef]
64. Siino, M.; Scudero, S.; Cannelli, V.; Piersanti, A.; D'Alessandro, A. Multiple Seasonality in Soil Radon Time Series. *Sci. Rep.* **2019**, *9*, 8610. [CrossRef]
65. Miklyaev, P.S.; Petrova, T.B.; Shchitov, D.V.; Sidyakin, P.A.; Murzabekov, M.A.; Tsebro, D.N.; Marennyy, A.M.; Nefedov, N.A.; Gavriliev, S.G. Radon Transport in Permeable Geological Environments. *Sci. Total Environ.* **2022**, *852*, 158382. [CrossRef] [PubMed]
66. Benkovitz, A.; Zafrir, H.; Reuveni, Y. A Novel Assessment of the Surface Heat Flux Role in Radon (Rn-222) Gas Flow within Subsurface Geological Porous Media. *Remote Sens.* **2023**, *15*, 4094. [CrossRef]
67. Mao, Y.; Zhang, L.; Wang, H.; Guo, Q. The Temporal Variation of Radon Concentration at Different Depths of Soil: A Case Study in Beijing. *J. Environ. Radioact.* **2023**, *264*, 107200. [CrossRef] [PubMed]
68. Rábago, D.; Quindós, L.; Vargas, A.; Sainz, C.; Radulescu, I.; Ioan, M.-R.; Cardellini, F.; Capogni, M.; Rizzo, A.; Celaya, S.; et al. Intercomparison of Radon Flux Monitors at Low and at High Radium Content Areas under Field Conditions. *Int. J. Environ. Res. Public Health* **2022**, *19*, 4213. [CrossRef] [PubMed]
69. Ryzhakova, N.K.; Stavitskaya, K.O.; Plastun, S.A. The Problems of Assessing Radon Hazard of Development Sites in the Russian Federation and the Czech Republic. *Radiat. Meas.* **2022**, *150*, 106681. [CrossRef]
70. Rizo Maestre, C.; Echarri Iribarren, V. The Radon Gas in Underground Buildings in Clay Soils. The Plaza Balmis Shelter as a Paradigm. *Int. J. Environ. Res. Public Health* **2018**, *15*, 1004. [CrossRef] [PubMed]
71. Shweikani, R.; Giaddui, T.G.; Durrani, S.A. The Effect of Soil Parameters on the Radon Concentration Values in the Environment. *Radiat. Meas.* **1995**, *25*, 581–584. [CrossRef]
72. Ciotoli, G.; Lombardi, S.; Zarlenga, F. Natural leakage of helium from Italian sedimentary basins of the Adriatic structural margin. In Proceedings of the Advances in the Geological Storage of Carbon Dioxide; Lombardi, S., Altunina, L.K., Beaubien, S.E., Eds.; Springer: Dordrecht, The Netherlands, 2006; pp. 191–202.
73. Ciotoli, G.; Lombardi, S.; Annunziatellis, A. Geostatistical Analysis of Soil Gas Data in a High Seismic Intermontane Basin: Fucino Plain, Central Italy. *J. Geophys. Res. Solid Earth* **2007**, *112*, B05407. [CrossRef]
74. Berberich, G.M.; Berberich, M.B. Comparison of Geogases in Two Cenozoic Sedimentary Basins. *Geosciences* **2022**, *12*, 388. [CrossRef]

Disclaimer/Publisher's Note: The statements, opinions and data contained in all publications are solely those of the individual author(s) and contributor(s) and not of MDPI and/or the editor(s). MDPI and/or the editor(s) disclaim responsibility for any injury to people or property resulting from any ideas, methods, instructions or products referred to in the content.